Chemical Physics Letters 804 (2022) 139876

Contents lists available at ScienceDirect

Chemical Physics Letters

journal homepage: www.elsevier.com/locate/cplett

Near-Infrared photodetectors based on 2D Bi_2S_3

Basant Chitara [a], Bhargava S.C. Kolli [b], Fei Yan [a,*]

[a] Department of Chemistry and Biochemistry, North Carolina Central University, Durham, NC 27707, USA
[b] Department of Biology, University of Florida, Gainesville, FL 32611, USA

ARTICLE INFO

Keywords:
CVD
2D Bi_2S_3
NIR photodetectors

ABSTRACT

Herein, we report for the first time, the chemical vapor deposition of 2D bismuth sulfide (Bi_2S_3). The 2D Bi_2S_3-based field-effect transistor showed an n-type electron mobility of 12.5 $cm^{-2}V^{-1}s^{-1}$ with an on/off ratio of 10. Under 785 nm illumination, the 2D Bi_2S_3-based photodetector exhibited a photo responsivity of 16 AW^{-1}, an external quantum efficiency of 2500%, a detectivity in the order of 10^{10} Jones and a linear dynamic range of 35 dB with a fast response time of 100 ms. Our results suggest that Bi_2S_3 could be a promising new 2D material for the next-generation electronic and optoelectronic devices.

1. Introduction

The discovery of graphene has opened the door to explore a wide variety of 2D materials for the next-generation ultrathin electronics and optoelectronics device applications. The ultrathin nature of these 2D materials brings scalability, smooth interfaces, and higher surface area [1]. Moreover, the natural passivation of 2D materials offers special advantage of stacking different 2D materials to create tunable van der Waals heterostructures [2]. The realization of such heterostructures in conventional 3D materials requires high-cost technology to create epitaxial heterostructures [3]. The lower dimensionality leads to higher optical response due to a prolonged carrier lifetime as a result of quantum confinement in contrast to their bulk counterparts, however, devices made from 0D quantum dot films suffer from severe scattering effects due to various grain boundaries, resulting in poor electrical performance (i.e., low carrier mobility). Moreover, the incomplete surface coverage [4] in 1D materials makes 2D material a convincing alternate for flexile optoelectronic devices application requiring ultra-thinness, low-cost, portability, and mechanical stability with high performance [5].

One such application of these ultrathin 2D materials is for infrared (IR) photodetection. IR photodetectors have been extensively employed for thermal imaging, biomedical imaging, night vision, information communication, and military etc [6–8]. The bandgap in semiconducting materials is the crucial factor for determining the photodetection wavelength. Silicon [9] and germanium [10] have always been the first choices for NIR photodetection but these materials face significant challenges where the bendability is desired in optoelectronics [11]. This has motivated the scientific community to look for new materials offering high mechanical strength, wide bandgap tunability and low-cost processability for IR photodetection applications. In this context, 2D materials due to their excellent electronic [6,12–14] and mechanical properties [15–17] seem to be suitable candidates for large-area and low-cost IR photodetecting applications. Various 2D materials have already been exploited for IR photodetectors, these include graphene, [6] transition metal dichalcogenides (TMDs) [8,18] and black phosphorus (BP) [19–21]. Unfortunately, graphene [6,22] suffers from low light absorption and TMDs have issues with air stability needing encapsulation [23,24] and/or functionalization [25], BP [26] and MXenes [25] suggest towards exploration of new 2D materials.

Bi_2S_3, an environmentally benign n-type 2D material emerges as a potential candidate for such applications due to its direct bandgap (1.3 – 1.7 eV) [27] and large absorption coefficient for photodetecting application [28]. It is a typical lamella-structured chalcogenide semiconductor exhibiting an orthorhombic crystal structure with Pnma space group [28]. Bi_2S_3 belongs to the stibnite family, is an anisotropic layered material exhibiting interesting optoelectronic properties due to strong spin–orbit coupling. In addition, the small effective carrier mass and the low thermal conductivity in Bi_2S_3 result in excellent thermoelectric properties. The thickness-dependent direct bandgap in Bi_2S_3 could be tailored between 1.3 eV and 1.7 eV, making 2D Bi_2S_3 a promising candidate for optoelectronic applications in the NIR spectrum. 0D Bi_2S_3 nanodots/particles, 1D Bi_2S_3 nanorods/nanowires/nanotubes, [29] or 3D Bi_2S_3 hierarchical architectures have been extensively exploited for photodetecting applications. However, due to the challenge of synthesizing 2D Bi_2S_3, there is limited literature [30] on photodetecting

* Corresponding author.
E-mail addresses: bchitara@nccu.edu (B. Chitara), fyan@nccu.edu (F. Yan).

https://doi.org/10.1016/j.cplett.2022.139876
Received 18 June 2022; Received in revised form 3 July 2022; Accepted 12 July 2022
Available online 16 July 2022
0009-2614/© 2022 Elsevier B.V. All rights reserved.

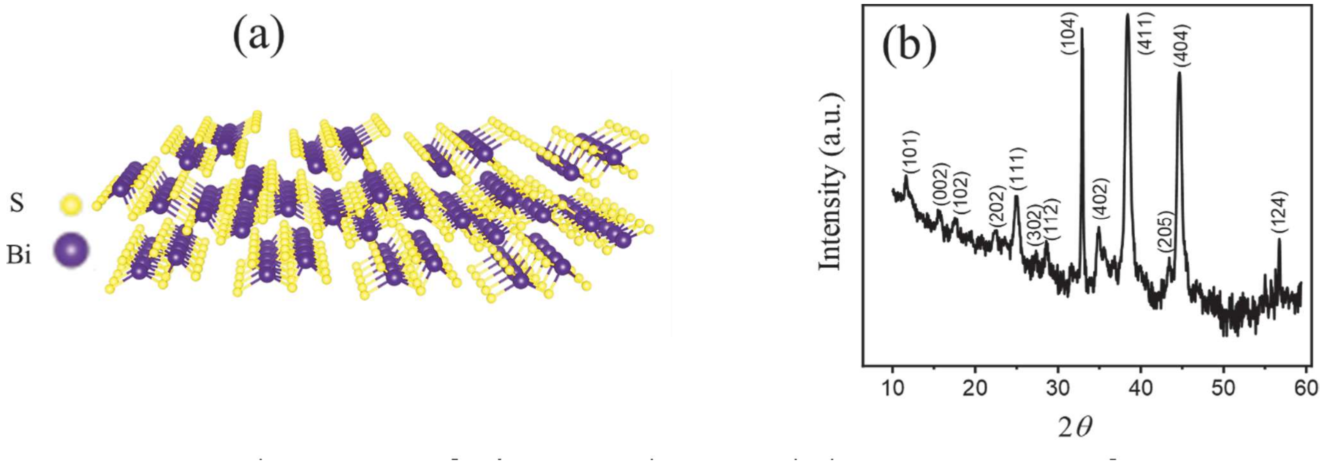

Fig. 1. (a) Crystal structure of Bi_2S_3 nanosheets, and (b) XRD pattern of CVD-grown 2D Bi_2S_3 thin film.

applications based on 2D Bi_2S_3. The difficulty in synthesizing 2D Bi_2S_3 stems from its highly anisotropic orthorhombic phase consisting of infinite ribbon-like Bi_4S_6 polymers linked together by intermolecular attraction between Bi and S atoms. The chain-like building blocks are parallel to the c-axis which make them preferential growth into 1D nanostructure along [0 0 1] direction [31]. As a result, it is very challenging and significant to explore the synthesis and optoelectronic application of ultrathin Bi_2S_3 nanosheets. Various synthetic routes have been employed to grow 2D Bi_2S_3 such as hydrothermal synthesis, [32] sol–gel methods, chemical bath deposition, [33] physical vapor deposition techniques and so on [28]. Here we report for the first time CVD growth of 2D Bi_2S_3 for NIR photodetection. In the present investigation, ultrathin freestanding Bi_2S_3 thin films have been synthesized by CVD in contrast to hydrothermal and chemical bath deposition reported in literature.

2. Experimental details

For the CVD growth of 2D Bi_2S_3, we have modified a previous method designed for the solution-processed synthesis of bismuth oxyselenide (Bi_2O_2Se) thin film reported by Zhang *et al.* [34]. The synthesis of 2D Bi_2S_3 is a two-step process. In the first step, 2D Bi_2O_3 is obtained over fluorphlogopite mica (f-mica) followed by sulfurization, which eventually leads to the formation of Bi_2S_3 film. Briefly, the CVD growth of 2D Bi_2S_3 was carried out by dissolving 1 g $Bi(NO_3)_3{\cdot}5H_2O$ in 10 mL ethylene glycol $(CH_2OH)_2$ to form a colorless transparent solution. The resultant solution was spin-coated onto freshly cleaved f-mica at 2000 rpm for 40 sec followed by heating at 180 °C for 30 sec. Subsequently, the $Bi(NO_3)_3$ thin film converted into Bi_2O_3 thin film by heating it at 480 °C for 30 min in air at a rate of ~ 8 °C/min. The final Bi_2S_3 thin film was obtained via sulfurization of Bi_2O_3 thin film. This was achieved by placing sulfur powder (100 mg) upstream at a distance of 15 cm from the Bi_2O_3 thin film which was kept downstream in a 45-mm diameter quartz tube. The CVD was performed at 200 ^{0}C for sulfur and 450 ^{0}C for Bi_2O_3 with an Argon flow of 200 sccm under a pressure of 500 mbar. The same steps were repeated for growing Bi_2S_3 films over SiO_2/Si substrates.

PANalytical X'Pert Pro MRD HR XRD System was used to obtain the X-ray diffraction data for determining the crystal structure of 2D Bi_2S_3. Raman spectra and Atomic Force Microscopy (AFM) maps of CVD-grown Bi_2S_3 were observed using a HORIBA LabRAM Evolution RAMAN microscope-Smart SPM atomic force microscope with a 532 nm laser. The UV–Vis-NIR absorption spectrum of 2D Bi_2S_3 was obtained by employing UV 3000 spectrophotometer. TEM characterization was performed using a ThermoFisher Titan 80–300 probe aberration corrected scanning transmission electron microscope (STEM) with a monochromator operating at 80–300 kV. CVD-grown 2D Bi_2S_3 thin films over mica were transferred over Cu TEM grids via the polystyrene (PS)-assisted transfer method [35].

The field-effect transistor (FET) device was fabricated via transferring 2D Bi_2S_3 over patterned gold electrode (purchased from Amazon) over Si with a 300-nm thick oxide layer. The distance between the two fingers was 20 μm and the width of each finger was 30 μm. The length of the finger was~1400 μm. Briefly, PS was spin coated over f-mica substrates containing Bi_2S_3 at 3000 rpm. for 60 s followed by baking at 85 °C for 15 min. Thereafter, a drop of DI water was used to peel off the PS-coated Bi_2S_3-film from f-mica. Consequently, PS-Bi_2S_3 film floating over water was transferred over patterned electrodes by carefully placing the PS-Bi_2S_3 film over the electrodes. Next, the device

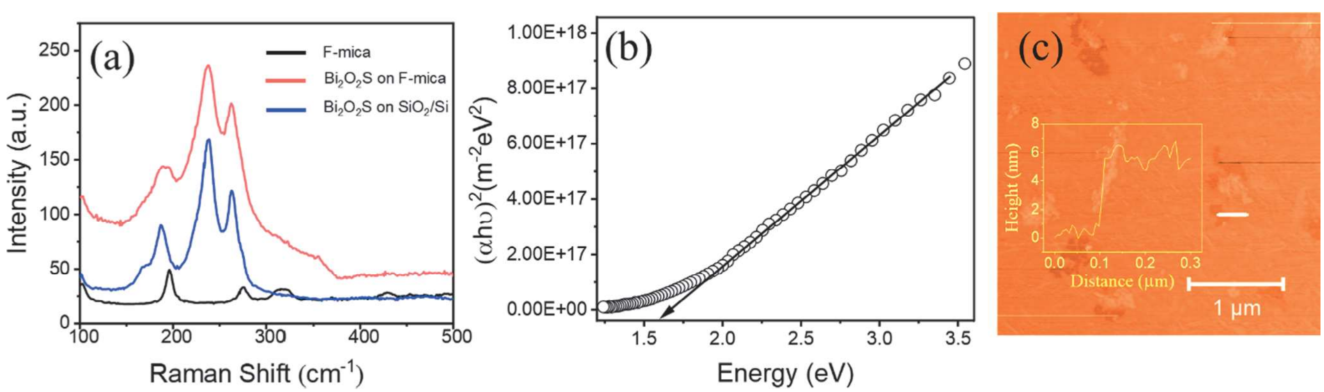

Fig. 2. (a) Raman spectra of 2D Bi_2S_3 grown on two different substrates, (b) UV–Vis-NIR spectrum of 2D Bi_2S_3, and (c) AFM image of CVD-grown 2D Bi_2S_3. Scale bar: 1 μm.

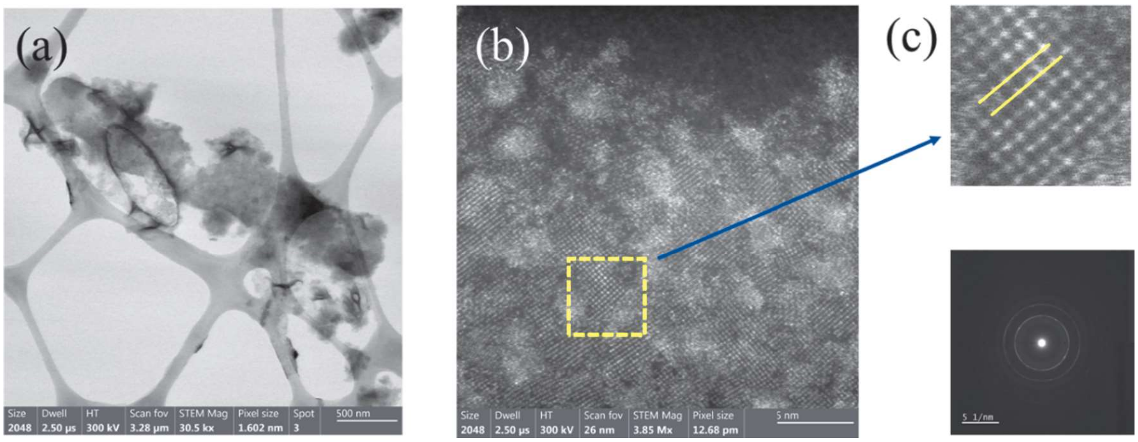

Fig. 3. (a) Bright field TEM image of CVD grown Bi_2S_3 with SAED shown as inset. Scale bar: 500 nm. (b) STEM of Bi_2S_3 domains merged together with different in-plane orientations. Scale bar: 5 nm. (c) Magnified STEM image illustrating the observed crystal spacing (upper image) and SAED pattern of a synthesized nanosheet (lower image). Scale bar: 5 nm^{-1}.

with PS-Bi_2S_3 film was then heated at 150 °C for 30 min to improve the contact between the sample and the underlying substrate. Finally, the PS layer was dissolved by keeping the device in toluene for overnight followed by acetone treatment for 1 h to remove the organic residuals. The FET device was dried using a nitrogen gun.

NIR photodetectors with dimensions of 25 µm length and ~ 1.5 mm width were realized via thermally evaporating Ti (5 nm)/Au (200 nm) over SiO_2/Si substrates containing Bi_2S_3 using a shadow mask. The electrical properties of the FET and NIR photodetectors were measured using Keysight B2902A Precision Source/Measure Unit with C-2 Mini Station (Everbeing Int'l corp.) HORIBA LabRAM Evolution RAMAN Microscope-Smart SPM Atomic Force Microscope equipped with 785 nm laser was used as the light source in the present study. The intensity of the laser was calculated using a calibrated Si photodiode. The difference between the current under illumination and the dark corresponds to the photocurrent.

3. Results and discussion

Fig. 1(a) illustrates the schematic crystal structure of 2D Bi_2S_3 nanosheets where Bi^{3+} and S^{2+} are arranged one on top of the other in infinite chains, which are directed along the [0 0 1] axis in an orthorhombic cell structure. Fig. 1(b) represents the typical XRD pattern of CVD synthesized Bi_2S_3 thin film corresponding to the orthorhombic Pbnm space group (JCPDS No. 75–1306). The synthesis of Bi_2S_3 films takes place via the following reactions:

$$4Bi(NO_3)_3 \cdot 5H_2O \rightarrow 2Bi_2O_3 + 12NO_2(g) + 3O_2(g) + 20H_2O \quad (1)$$

$$2Bi_2O_3 + 9S(g) \rightarrow 2Bi_2S_3 + 3SO_2(g) \quad (2)$$

Fig. 2(a) displays the Raman spectrum of CVD-grown 2D Bi_2S_3 acquired using the 633 nm laser showing Raman intensity peaks at about 187, 236, and 260.3 cm^{-1}, which were in accordance with Raman peaks of Bi_2S_3 nanowires.[36] We have compared the Raman spectrum of Bi_2S_3/f-mica with those from Bi_2S_3/SiO_2/Si, and f-mica. The Raman spectra of both Bi_2S_3/f-mica and Bi_2S_3/SiO_2/Si were quite similar, confirming that we were able to grow 2D Bi_2S_3 over SiO_2 substrates, a much-needed growth condition required for transfer-free growth of 2D Bi_2S_3.

The devices can be easily realized without transferring the films in case of Bi_2S_3 grown over mica substrates. For this reason, we have fabricated the photodetecting devices from 2D Bi_2S_3 thin films over SiO_2 substrates. The optical band gap of CVD Bi_2S_3 was estimated using Tauc plot as shown in Fig. 2(b). The absorption coefficient α and optical band gap E_g are related through the Tauc relation [37] given by $(\alpha h\upsilon)^2 = B(h\upsilon - Eg)$ where h is Planck's constant, B is the energy-independent constant, and υ is the frequency of the incident photon. The bandgap of Bi_2S_3 in present study was estimated to be around 1.6 eV. Fig. 2(c) shows the AFM image of the 2D Bi_2S_3 with the corresponding height profile shown as inset. The thickness of Bi_2S_3 is around 5 nm thus confirming the ultrathin nature of 2D Bi_2S_3 nanosheets.

Fig. 3(a) shows a TEM image of 2D Bi_2S_3 for investigating the nanosheet morphology. We performed top-view TEM characterizations of the as-synthesized 2D Bi_2S_3 by transferring it onto a holey carbon

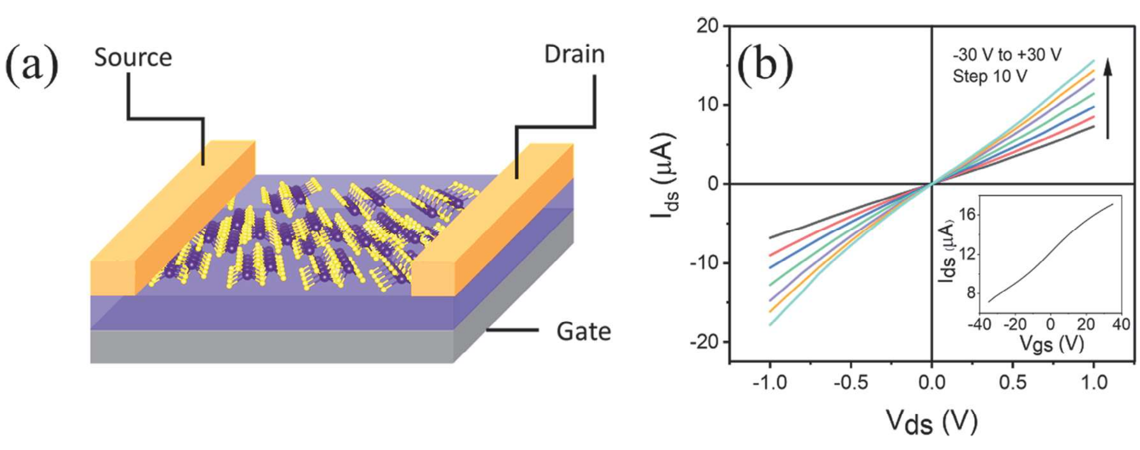

Fig. 4. (a) Schematic of a 2D Bi_2S_3-based FET, (b) Output characteristics, and c) Transfer characteristics of a 2D Bi_2S_3-based FET device.

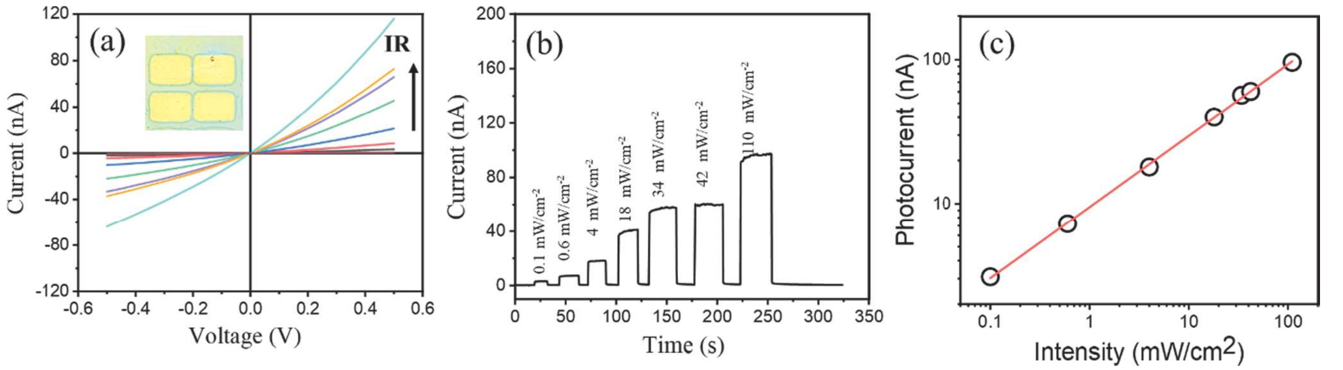

Fig. 5. (a) Current-voltage (I-V) characteristics of 2D Bi_2S_3-based photodetector under dark and under different illumination at 785 nm. Inset: The optical image of the photodetector. (b) Current-time (I-t) characteristics of the device under dark and 785 nm with varying light intensity. (c) Photocurrent measured as a function of incident light density at a bias voltage of 0.5 V. The empty circles are the experimental points, and the solid line is a linear fit to the data.

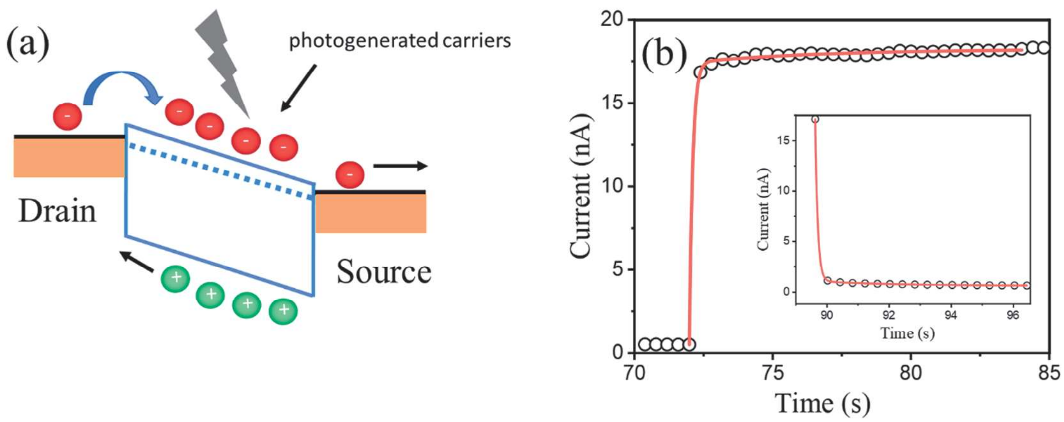

Fig. 6. (a) Photodetection mechanism for 2D Bi_2S_3 device. (b) Time response of photocurrent growth and decay (in insets) for Bi_2S_3 photodetector. The empty circles are the experimental points, and the solid lines are fits to the exponential equations.

supported Cu grid. Fig. 3(b) depicts the STEM image showing domains with different crystal orientations merge together with a lattice spacing of 0.32 nm. Fig. 3(c) illustrates the magnified STEM image (upper image) and the selected area electron diffraction (SAED) pattern (lower image) of the as-grown 2D Bi_2S_3. The presence of several sets of diffraction patterns on a ring suggests the polycrystalline nature of CVD-grown 2D Bi_2S_3 thin films.

To explore the electronic application of 2D Bi_2S_3, we have investigated the output and transfer characteristics of 2D Bi_2S_3-based FET. Fig. 4(a) shows the schematic diagram of a 2D Bi_2S_3-based FET. Fig. 4(b) demonstrates the output characteristics of Bi_2S_3 nanosheet FET device with inset showing the transfer characteristics of 2D Bi_2S_3 based FET. The device exhibited a typical n-type transfer characteristic with an on/off ratio of ~ 10. The electron mobility was estimated using $\mu = L/W*1/C_{ox}*dI_{ds}/dV_{bg}*1/V_{ds}$ from transconductance vs back-gate voltage (V_{bg}) in the range of $-35\ V < V_{bg} < 35\ V$, where L is the length of the channel, W is the channel width, C_{ox} is the capacitance of 300 nm SiO_2, dI_{ds}/dV_{bg} is the measured transconductance of the channel, and V_{bg} is the back-gate voltage.

The dielectric capacitance C_{ox} can be obtained via $C_{ox} = \varepsilon_0\varepsilon r/d_{ox}$, where the oxide thickness d_{ox} is around 300 nm, the relative permittivity ε_r of SiO_2 is 3.9, and the free space permittivity ε_0 is $8.87 \times 10^{-12} F\ m^{-1}$. The mobility of the as-grown 2D Bi_2S_3 was determined to be about 12.4 $cm^2\ V^{-1}\ s^{-1}$ at room temperature, which is comparable to that of other 2D materials such as GaS, [38] MoS_2, [39] ReS_2, [40] and In_2S_3 [41].

The NIR photoconducting response (under 785 nm) of the CVD-grown 2D Bi_2S_3 with varying light intensity is presented in Fig. 5(a) with an optical image of the photodetector shown as inset. Fig. 5(b) demonstrates the switching behavior of the photodetector under different light intensities. The stability and the reproducibility of the 2D Bi_2S_3-based photodetector were confirmed by switching on and off the NIR laser source. The electrical conductivity of the device increases with increasing light intensity. This can be attributed to the absorption of more photons resulting in a larger photocurrent. The variation of photocurrent vs intensity is plotted in Fig. 5(c).

The mechanism behind the photodetection is presented as inset in Fig. 6(a). Upon illuminating the device with a NIR light source, the absorption of the NIR light generates electron-hole pairs, [8,42,43] which in turn can be extracted on applying bias voltage across the device. The photoresponsivity, the external quantum efficiency (EQE), the detectivity (D*) and the time response of the photodetector play a crucial role in determining the application in commercial applications [8,44,45]. The photoresponsivity is defined corresponding to photocurrent generated per unit power of the incident light, the EQE, i.e. the number of electrons is detected per incident photon and the detectivity (D*) can be calculated as $R_\lambda = I_\lambda/P_\lambda S$, $EQE = hcR_\lambda/e\lambda$ and $D^* = (S\Delta f)^{1/2}/NEP$ respectively, where I_λ corresponds to photocurrent (I_{light}-I_{dark}), P_λ is the intensity of light, S is the device effective area under illumination, h is Planck's constant, e is the electronic charge, c is the velocity of the light, λ is the illumination wavelength, Δf is electrical bandwidth in Hz and *NEP* is the noise equivalent power. D^* can be deduced to $D^* = I_\lambda S^{1/2}/P_\lambda S(2eI_{dark})^{1/2}$ by assuming dark current to be the major contributor to the shot noise to get a fast approximation of the D* [46]. However, it is worth noting that by choosing shot noise as the major noise source overestimates the value of D^* [47,48].

According to our experimental results, R_λ and EQE of Bi_2S_3 are 16

Table 1
NIR detection performance of different 2D materials.

2D Materials	Wavelength (nm)	Photoresponsivity (AW^{-1})	Detectivity (Jones)	Response time	Reference
GeSe	808	3.5	–	100 ms	[50]
$SnSe_2$	1064	2×10^{-3}	2×10^{11}	0.38 s	[51]
Sb_2Te_3	980	21.7	1.2×10^{10}	238 s	[52]
SnS	808	1	10^{9}	–	[53]
Bi_2S_3	780	4.4	2×10^{11}	10 μs	[30]
Bi_2O_2S	785	4	2×10^{10}	100 ms	[3]
Bi_2S_3	785	16.5	10^{10}	100 ms	This work

AW^{-1} and 2500 %, respectively for an incident wavelength of 785 nm at 0.5 V. CVD-grown 2D Bi_2S_3 in the present study shows superior performance as compared to hydrothermally-grown 2D Bi_2S_3 nanosheets (a photoresponsivity 4.5 AW^{-1} and an EQE of 860%) [30] and 2D Bi_2S_3 nanosheets synthesized by a liquid metal-based technique (a photoresponsivity 8 AW^{-1}) [49]. The detectivity of 2D Bi_2S_3-based photodetectors was found to be in the order of 10^{10} Jones, which is much higher than those observed in graphene, BP, $MoTe_2$, Bi_2Se_3 and MoS_2 etc [3]. Moreover, the linear dynamic range (LDR) estimated by LDR = 20 log (I_{ph}/I_{dark}), where I_{ph} is the photocurrent, measured at a light intensity of 4 mW cm^{-2}. The LDR in 2D Bi_2S_3 was estimated to be 35.5 dB. All these results clearly demonstrate that CVD-grown 2D Bi_2S_3 can be a promising candidate for use as high-selectivity, high sensitivity, and high-speed nanometer-scale photodetectors and photoelectronic switches.

To investigate the time response to the IR illumination being turned on and off, we have shown photocurrent growth in Fig. 6(b) with decay response shown as inset. The transient photocurrent response of 2D Bi_2S_3 photodetector to NIR has been obtained via the following equations $I(t) = I_{dark} + A\,[\exp(-(t-t_o)/\tau_1)] + B\,[\exp(-(t-t_o)/\tau_2)]$ and $I(t) = I_{dark} + A\,[\exp(-(t-t_o)/\tau_1)] + B\,[\exp(-(t-t_o)/\tau_2)]$ for growth and decay, respectively, where τ is the time constant and t is the time when IR is switched on or off, I_{dark} is the dark current, and A and B are scaling constants. The experimental data has been presented as circles and a solid red line as the linear fit of the experimental data points. The time growth takes place via two-time constants where the 2D Bi_2S_3 photocurrent rises within 0.1 s followed by a slower time constant of 4.8 sec. On the other hand, the photocurrent decays abruptly within 0.02 sec with a slower time constant of 2 sec. We have compared the photodetection performance of our device with other 2D materials as depicted in Table 1. As evident from Table 1, the photodetection performance of our 2D Bi_2S_3-based photodetector is comparable to those made by other 2D materials.

4. Conclusion

To summarize, we demonstrate for the first time, large-area CVD growth of freestanding 2D Bi_2S_3 nanosheets and their utilization for high-performance NIR photodetection. A typical 2D Bi_2S_3 exhibits a thickness of ~ 5 nm. The as-grown 2D Bi_2S_3 exhibited a field-effect mobility of 12 cm^2V^{-1} s^{-1} which is comparable to some popular 2D materials such as MoS_2, GaS, GaSe, and WS_2 etc. The CVD-grown 2D Bi_2S_3-based NIR photodetector shows a photoresponsivity of 16 AW^{-1}, an EQE of 2500 %, a detectivity in the order of 10^{10} Jones, an LDR of 35.5 dB and a time response of 100 ms, which are comparable to those observed in other 2D materials-based IR detectors such as TMDs, BP, and Bi_2O_2Se etc. This study puts forward CVD-grown 2D Bi_2S_3 in conjugation with other 2D materials for exploitation in future optoelectronics over large areas.

CRediT authorship contribution statement

Basant Chitara: Conceptualization, Investigation, Writing – original draft, Data curation. **Bhargava S.C. Kolli**: Data curation. **Fei Yan:** Writing – review & editing, Validation, Supervision, Project administration, Funding acquisition.

Declaration of Competing Interest

The authors declare that they have no known competing financial interests or personal relationships that could have appeared to influence the work reported in this paper.

Acknowledgements

The authors are grateful for the financial support of this project by the U.S. National Science Foundation (Awards # 1831133 and #2122044). This work was performed in part at the Duke University Shared Materials Instrumentation Facility (SMIF), a member of the North Carolina Research Triangle Nanotechnology Network (RTNN), which is supported by the National Science Foundation (Grant ECCS-1542015) as part of the National Nanotechnology Coordinated Infrastructure (NNCI).

References

[1] Q.H. Wang, K. Kalantar-Zadeh, A. Kis, J.N. Coleman, M.S. Strano, Electronics and optoelectronics of two-dimensional transition metal dichalcogenides, Nat. Nanotechnol. 7 (11) (2012) 699–712.
[2] M. Long, P. Wang, H. Fang, W. Hu, Progress, Challenges, and Opportunities for 2D Material Based Photodetectors, Adv. Funct. Mater. 29 (2019) 1803807.
[3] B. Chitara, T.B. Limbu, J.D. Orlando, Y. Tang, F. Yan, Ultrathin Bi2O2S nanosheet near-infrared photodetectors, Nanoscale. 12 (30) (2020) 16285–16291.
[4] S. Akhavan, A.F. Cihan, B. Bozok, H.V. Demir, Nanocrystal Skins with Exciton Funneling for Photosensing, Small. 10 (12) (2014) 2470–2475.
[5] P. Hu, L. Wang, M. Yoon, J. Zhang, W. Feng, X. Wang, Z. Wen, J.C. Idrobo, Y. Miyamoto, D.B. Geohegan, K. Xiao, Highly Responsive Ultrathin GaS Nanosheet Photodetectors on Rigid and Flexible Substrates, Nano Lett. 13 (4) (2013) 1649–1654.
[6] C.-H. Liu, Y.-C. Chang, T.B. Norris, Z. Zhong, Graphene photodetectors with ultra-broadband and high responsivity at room temperature, Nat. Nanotechnol. 9 (4) (2014) 273–278.
[7] F. Wang, Y. Zhang, Y. Gao, P. Luo, J. Su, W. Han, K. Liu, H. Li, T. Zhai, 2D Metal Chalcogenides for IR Photodetection, Small. 15 (2019) 1901347.
[8] Z. Yin, H. Li, H. Li, L. Jiang, Y. Shi, Y. Sun, G. Lu, Q. Zhang, X. Chen, H. Zhang, Single-Layer MoS2 Phototransistors, ACS Nano 6 (1) (2012) 74–80.
[9] M.W. Geis, S.J. Spector, M.E. Grein, J.U. Yoon, D.M. Lennon, T.M. Lyszczarz, Silicon waveguide infrared photodiodes with >35 GHz bandwidth and phototransistors with 50 AW-1 response, Opt. Express. 17 (2009) 5193–5204.
[10] H.H. Tseng, H. Li, V. Mashanov, Y.J. Yang, H.H. Cheng, G.E. Chang, R.A. Soref, G. Sun, GeSn-based p-i-n photodiodes with strained active layer on a Si wafer, Appl. Phys. Lett. 103 (2013), 231907.
[11] N. Huo, G. Konstantatos, Recent Progress and Future Prospects of 2D-Based Photodetectors, Adv. Mater. 30 (2018) 1801164.
[12] K.S. Novoselov, A.K. Geim, S.V. Morozov, D. Jiang, Y. Zhang, S.V. Dubonos, I. V. Grigorieva, A.A. Firsov, Electric Field Effect in Atomically Thin Carbon Films, Science 306 (5696) (2004) 666–669.
[13] D.J. Late, B. Liu, H.S.S.R. Matte, V.P. Dravid, C.N.R. Rao, Hysteresis in Single-Layer MoS2 Field Effect Transistors, ACS Nano 6 (6) (2012) 5635–5641.
[14] D.J. Late, Y.-K. Huang, B. Liu, J. Acharya, S.N. Shirodkar, J. Luo, A. Yan, D. Charles, U.V. Waghmare, V.P. Dravid, C.N.R. Rao, Sensing Behavior of Atomically Thin-Layered MoS2 Transistors, ACS Nano 7 (6) (2013) 4879–4891.
[15] C. Lee, X. Wei, J.W. Kysar, J. Hone, Measurement of the Elastic Properties and Intrinsic Strength of Monolayer Graphene, Science 321 (5887) (2008) 385–388.
[16] B. Chitara, A. Ya'akobovitz, Elastic properties and breaking strengths of GaS, GaSe and GaTe nanosheets, Nanoscale. 10 (27) (2018) 13022–13027.
[17] K. Liu, Q. Yan, M. Chen, W. Fan, Y. Sun, J. Suh, D. Fu, S. Lee, J. Zhou, S. Tongay, J. Ji, J.B. Neaton, J. Wu, Elastic Properties of Chemical-Vapor-Deposited

Monolayer MoS2, WS2, and Their Bilayer Heterostructures, Nano Lett. 14 (9) (2014) 5097–5103.
[18] T.J. Octon, V.K. Nagareddy, S. Russo, M.F. Craciun, C.D. Wright, Fast High-Responsivity Few-Layer MoTe2 Photodetectors, Adv. Opt. Mater. 4 (11) (2016) 1750–1754.
[19] X. Chen, X. Lu, B. Deng, O. Sinai, Y. Shao, C. Li, S. Yuan, V. Tran, K. Watanabe, T. Taniguchi, D. Naveh, L. Yang, F. Xia, Widely tunable black phosphorus mid-infrared photodetector, Nat. Commun. 8 (2017) 1–7.
[20] X.i. Wang, W. Tian, M. Liao, Y. Bando, D. Golberg, Recent advances in solution-processed inorganic nanofilm photodetectors, Chem. Soc. Rev. 43 (5) (2014) 1400–1422.
[21] X. Yu, S. Zhang, H. Zeng, Q.J. Wang, Lateral black phosphorene P-N junctions formed via chemical doping for high performance near-infrared photodetector, Nano Energy 25 (2016) 34–41.
[22] F. Luo, M. Zhu, Y. tan, H. Sun, W. Luo, G. Peng, Z. Zhu, X.-A. Zhang, S. Qin, High responsivity graphene photodetectors from visible to near-infrared by photogating effect, AIP Adv. 8 (2018) 115106.
[23] Q. Li, Q. Zhou, L.i. Shi, Q. Chen, J. Wang, Recent advances in oxidation and degradation mechanisms of ultrathin 2D materials under ambient conditions and their passivation strategies, J. Mater. Chem. A. 7 (9) (2019) 4291–4312.
[24] L. Zhang, S. Shen, M. Li, L. Li, J. Zhang, L. Fan, F. Cheng, C. Li, M. Zhu, Z. Kang, J. Su, T. Zhai, Y. Gao, Strategies for Air-Stable and Tunable Monolayer MoS2-Based Hybrid Photodetectors with High Performance by Regulating the Fully Inorganic Trihalide Perovskite Nanocrystals, Adv. Opt. Mater. 7 (2019) 1801744.
[25] T.B. Limbu, B. Chitara, J.D. Orlando, M.Y. Garcia Cervantes, S. Kumari, Q.i. Li, Y. Tang, F. Yan, Green Synthesis of Reduced Ti3C2Tx MXene Nanosheets with Enhanced Conductivity, Oxidation Stability, and SERS Activity, J. Mater. Chem. C. 8 (14) (2020) 4722–4731.
[26] Q. Zhou, Q. Chen, Y. Tong, J. Wang, Light-Induced Ambient Degradation of Few-Layer Black Phosphorus: Mechanism and Protection, Angew. Chem. Int. Ed. 55 (38) (2016) 11437–11441.
[27] A. Begum, A. Hussain, A. Rahman, Optical and Electrical Properties of Doped and Undoped Bi2S3)-PVA Films Prepared by Chemical Drop Method, Mater. Sci. Appl. 2 (2011) 163–168.
[28] T.O. Ajiboye, D.C. Onwudiwe, Bismuth sulfide based compounds: Properties, synthesis and applications, Results Chem. 3 (2021), 100151.
[29] F. Lu, R. Li, Y. Li, N. Huo, J. Yang, Y. Li, B.o. Li, S. Yang, Z. Wei, J. Li, Improving the Field-Effect Performance of Bi2S3 Single Nanowires by an Asymmetric Device Fabrication, ChemPhysChem 16 (1) (2015) 99–103.
[30] G. Chen, Y. Yu, K. Zheng, T. Ding, W. Wang, Y. Jiang, Q. Yang, Fabrication of Ultrathin Bi2S3 Nanosheets for High-Performance, Flexible, Visible–NIR Photodetectors, Small. 11 (24) (2015) 2848–2855.
[31] D. Wang, C. Hao, W. Zheng, X. Ma, D. Chu, Q. Peng, Y. Li, Bi2S3 nanotubes: Facile synthesis and growth mechanism, Nano Res. 2 (2009) 130–134.
[32] M.-A. Shahbazi, L. Faghfouri, M.P.A. Ferreira, P. Figueiredo, H. Maleki, F. Sefat, J. Hirvonen, H.A. Santos, The versatile biomedical applications of bismuth-based nanoparticles and composites: therapeutic, diagnostic, biosensing, and regenerative properties, Chem. Soc. Rev. 49 (2020) 1253–1321.
[33] M.E. Rincón, P.K. Nair, Low-temperature vapour phase deposition of bismuth sulphide films, Semicond. Sci. Technol. 12 (4) (1997) 467–474.
[34] C. Zhang, J. Wu, Y. Sun, C. Tan, T. Li, T. Tu, Y. Zhang, Y. Liang, X. Zhou, P. Gao, H. Peng, High-Mobility Flexible Oxyselenide Thin-Film Transistors Prepared by a Solution-Assisted Method, J. Am. Chem. Soc. 142 (6) (2020) 2726–2731.
[35] A. Gurarslan, Y. Yu, L. Su, Y. Yu, F. Suarez, S. Yao, Y. Zhu, M. Ozturk, Y. Zhang, L. Cao, Surface-Energy-Assisted Perfect Transfer of Centimeter-Scale Monolayer and Few-Layer MoS2 Films onto Arbitrary Substrates, ACS Nano 8 (11) (2014) 11522–11528.
[36] Y. Li, L. Huang, B. Li, X. Wang, Z. Zhou, J. Li, Z. Wei, Co-nucleus 1D/2D Heterostructures with Bi2S3 Nanowire and MoS2 Monolayer: One-Step Growth and Defect-Induced Formation Mechanism, ACS Nano 10 (2016) 8938–8946.
[37] J. Tauc, R. Grigorovici, A. Vancu, Optical Properties and Electronic Structure of Amorphous Germanium, Phys. Status Solidi B. 15 (2) (1966) 627–637.
[38] D.J. Late, B. Liu, J. Luo, A. Yan, H.S.S.R. Matte, M. Grayson, C.N.R. Rao, V. P. Dravid, GaS and GaSe Ultrathin Layer Transistors, Adv. Mater. 24 (26) (2012) 3549–3554.
[39] H.-W. Tu, C.-C. Shih, C.-L. Lin, M.-Z. Yu, J.-J. Lai, J.-C. Luo, G.-L. Lin, W.-B. Jian, K. Watanabe, T. Taniguchi, C. Hu, High field-effect performance and intrinsic scattering in the two-dimensional MoS2 semiconductors, Appl. Surf. Sci. 564 (2021), 150422.
[40] B. Jariwala, D. Voiry, A. Jindal, B.A. Chalke, R. Bapat, A. Thamizhavel, M. Chhowalla, M. Deshmukh, A. Bhattacharya, Synthesis and Characterization of ReS2 and ReSe2 Layered Chalcogenide Single Crystals, Chem. Mater. 28 (10) (2016) 3352–3359.
[41] A. Jannat, Q. Yao, A. Zavabeti, N. Syed, B.Y. Zhang, T. Ahmed, S. Kuriakose, M. d. Mohiuddin, N. Pillai, F. Haque, G. Ren, D.M. Zhu, N. Cheng, Y.i. Du, S.A. Tawfik, M.J.S. Spencer, B.J. Murdoch, L. Wang, C.F. McConville, S. Walia, T. Daeneke, L. Zhu, J.Z. Ou, Ordered-vacancy-enabled indium sulphide printed in wafer-scale with enhanced electron mobility, Mater. Horiz. 7 (3) (2020) 827–834.
[42] J. Li, Z. Wang, Y. Wen, J. Chu, L. Yin, R. Cheng, L. Lei, P. He, C. Jiang, L. Feng, J. He, High-Performance Near-Infrared Photodetector Based on Ultrathin Bi $_2$ O $_2$ Se Nanosheets, Adv. Funct. Mater. 28 (2018) 1706437.
[43] PingAn Hu, Z. Wen, L. Wang, P. Tan, K. Xiao, Synthesis of Few-Layer GaSe Nanosheets for High Performance Photodetectors, ACS Nano 6 (7) (2012) 5988–5994.
[44] Q. Fu, C. Zhu, X. Zhao, X. Wang, A. Chaturvedi, C. Zhu, X. Wang, Q. Zeng, J. Zhou, F. Liu, B.K. Tay, H. Zhang, S.J. Pennycook, Z. Liu, Ultrasensitive 2D Bi $_2$ O $_2$ Se Phototransistors on Silicon Substrates, Adv. Mater. 31 (2019) 1804945.
[45] P. Luo, F. Zhuge, F. Wang, L. Lian, K. Liu, J. Zhang, T. Zhai, PbSe Quantum Dots Sensitized High-Mobility Bi2O2Se Nanosheets for High-Performance and Broadband Photodetection Beyond 2 μm, ACS Nano 13 (8) (2019) 9028–9037.
[46] J. Li, Z. Wang, Y. Wen, J. Chu, L. Yin, R. Cheng, L. Lei, P. He, C. Jiang, L. Feng, J. He, High-Performance Near-Infrared Photodetector Based on Ultrathin Bi2O2Se Nanosheets, Adv. Funct. Mater. 28 (2018) 1706437.
[47] Y. Zhang, D.J. Hellebusch, N.D. Bronstein, C. Ko, D.F. Ogletree, M. Salmeron, A. P. Alivisatos, Ultrasensitive photodetectors exploiting electrostatic trapping and percolation transport, Nat. Commun. 7 (2016) 11924.
[48] D. Kufer, G. Konstantatos, Highly Sensitive, Encapsulated MoS2 Photodetector with Gate Controllable Gain and Speed, Nano Lett. 15 (11) (2015) 7307–7313.
[49] K.A. Messalea, A. Zavabeti, M. Mohiuddin, N. Syed, A. Jannat, P. Atkin, T. Ahmed, S. Walia, C.F. McConville, K. Kalantar-Zadeh, N. Mahmood, K. Khoshmanesh, T. Daeneke, Two-Step Synthesis of Large-Area 2D Bi2S3 Nanosheets Featuring High In-Plane Anisotropy, Adv. Mater. Interfaces. 7 (2020) 2001131.
[50] B. Mukherjee, Y. Cai, H.R. Tan, Y.P. Feng, E.S. Tok, C.H. Sow, NIR Schottky Photodetectors Based on Individual Single-Crystalline GeSe Nanosheet, ACS Appl. Mater. Interfaces. 5 (19) (2013) 9594–9604.
[51] E.P. Mukhokosi, S.B. Krupanidhi, K.K. Nanda, Band Gap Engineering of Hexagonal $SnSe_2$ Nanostructured Thin Films for Infra-Red Photodetection, Sci. Rep. 7 (2017) 15215.
[52] K. Zheng, L.-B. Luo, T.-F. Zhang, Y.-H. Liu, Y.-Q. Yu, R. Lu, H.-L. Qiu, Z.-J. Li, J. C. Andrew Huang, Optoelectronic characteristics of a near infrared light photodetector based on a topological insulator Sb2Te3 film, J. Mater. Chem. C. 3 (35) (2015) 9154–9160.
[53] J. Yao, G. Yang, Flexible and High-Performance All-2D Photodetector for Wearable Devices, Small. 14 (2018) 1704524.